Ecological and hydroclimate responses to strengthening of the Hadley circulation in South America during the Late Miocene cooling

Barbara Carrapa[a,1], Mark Clementz[b], and Ran Feng[c]

[a]Department of Geosciences, University of Arizona, Tucson, AZ 85721; [b]Department of Geology and Geophysics, University of Wyoming, Laramie, WY 82071; and [c]Department of Geosciences, University of Connecticut, Storrs, CT 06269

Edited by Gilles Ramstein, Commissariat à l'Énergie Atomique et aux Énergies Alternatives - CNRS - Universite de Versailles Saint-Quentin, Gif-Sur-Yvette, France, and accepted by Editorial Board Member Jean Jouzel March 27, 2019 (received for review June 22, 2018)

Near-modern ecosystems were established as a result of rapid ecological adaptation and climate change in the Late Miocene. On land, Late Miocene aridification spread in tandem with expansion of open habitats including C_4 grassland ecosystems. Proxy records for the central Andes spanning the Late Miocene cooling (LMC) show the reorganization of subtropical ecosystems and hydroclimate in South America between 15 and 35°S. Continental pedogenic carbonates preserved in Neogene basins record a general increase of $\delta^{18}O$ and $\delta^{13}C$ values from pre-LMC to post-LMC, most robustly occurring in the subtropics (25 to 30°S), suggesting aridification and a shift toward a more C4-plant-dominated ecosystem. These changes are closely tied to the enhancement of the Hadley circulation and moisture divergence away from the subtropics toward the Intertropical Convergence Zone as revealed by climate model simulations with prescribed sea-surface temperatures (SSTs) reflecting different magnitudes of LMC steepening of equator-to-pole temperature gradient and CO_2 decline.

Late Miocene cooling | South America | Hadley circulation | stable isotopes | Andes

The Miocene marks the establishment of near-modern ecosystems, which are characterized by moderate atmospheric CO_2 concentrations (ranging from ∼200 to 300 ppm during the Late Miocene to above 400 ppm during the Early and Mid-Miocene) (1, 2) and the expansion of grassland biomes (3, 4). The transition from greenhouse conditions of the Paleogene to an increasingly near-modern climate state in the Miocene was punctuated by two episodes of global climatic variation characterized by clear shifts in stable isotope data from oceanic sedimentary records: the Middle Miocene climatic optimum (MMCO) and the Late Miocene cooling (LMC). Whereas the MMCO has been recognized for some time, the significance of the LMC is still being assessed, especially on the continent. The LMC is associated with an ∼6 °C decrease in SST from 7 to 5.4 Ma across the high latitudes (30–50° N/S) (3); by Early Pliocene time SSTs were similar to today (5). CO_2 reconstructions fail to show appreciable changes in CO_2 concentration potentially attributable to the lack of high-resolution records or method limitation (2). Nonetheless, radiative forcing associated with CO_2 decline remains the leading hypothesis to explain the LMC (3).

We focus on the central Andes (Fig. 1) because their tectonosedimentary history is well constrained (6); combined with a wealth of geochemical data, this provides a unique opportunity to reconstruct paleoclimate across South America. Relationships between climate and vegetation have long been studied; the global expansion of C_4 plants has been linked to declining global temperatures and CO_2 concentrations since the Late Oligocene (4). Expansion of C_4 plants at ∼8 Ma in the central Andes has been connected to an increase in seasonality (7). Prior records of Cenozoic grassland appearance and expansion in South America have primarily relied on the mammalian fossil record (8–10), which shows an increase in C_4 contribution to herbivore diets in the Late Miocene (Fig. 2*A*) and an increasing abundance of species with high-crowned (hypsodont) or ever-growing (hypselodont) dentitions over time (Fig. 2*B*). In North America, this morphology has been cited as evidence of the spread of grasslands during the Miocene (11), but hypsodont and hypselodont species appear much earlier in South America (Middle Eocene, ∼40 Ma) (12), raising the possibility that open habitats resulting from early aridification in the southern Andes may have controlled faunal evolution (13, 14).

A key time interval for understanding Neogene climate and ecosystem evolution across South America is the LMC event (3), which coincides with global records of lower $\delta^{13}C$ values in marine carbonates (3, 15) and a general increase in soil carbonate $\delta^{13}C$. The latter is proposed to reflect an expansion of C_4 grasses in North America, Asia, Africa, and South America (8, 16). These shifts suggest potential perturbation in the carbon cycle at global scale. Nonetheless, signals of continental ecosystem changes show that heterogeneous changes across the LMC are embedded in the Late Neogene long-term global climate cooling trend, which has hindered the reconstruction and understanding of spatial structure of continental climate during the LMC.

We compile available $\delta^{18}O$ and $\delta^{13}C$ records from pedogenic carbonates preserved in several basins along the central Andes, between ∼15 and 35°S, and combine this analysis with general circulation model simulations (Figs. 1 and 2). $\delta^{18}O$ and $\delta^{13}C$ of

Significance

This paper analyzes the Late Miocene continental record of hydroclimate from the central Andes and subsequent ecological response to climatic change during this interval. The Late Miocene cooling (LMC) is characterized by a sharp decrease (up to 6 °C) of sea-surface temperatures and has been shown to have driven ecosystem reorganization, leading to conditions similar to Quaternary. We use the stable isotopic record preserved in pedogenic carbonate nodules as a proxy for hydroclimate changes during the LMC. This, combined with general circulation simulations, shows that strengthening of the Hadley circulation in South America during the LMC enhanced subtropical aridification and in turn promoted expansion of C_4 grasses and evolution of high-crowned teeth in mammals.

Author contributions: B.C. designed research; B.C., M.C., and R.F. performed research; B.C., M.C., and R.F. analyzed data; and B.C., M.C., and R.F. wrote the paper.

The authors declare no conflict of interest.

This article is a PNAS Direct Submission. G.R. is a guest editor invited by the Editorial Board.

[1]To whom correspondence should be addressed. Email: bcarrapa@email.arizona.edu.

This article contains supporting information online at www.pnas.org/lookup/suppl/doi:10.1073/pnas.1810721116/-/DCSupplemental.

Published online April 29, 2019.

EARTH, ATMOSPHERIC, AND PLANETARY SCIENCES

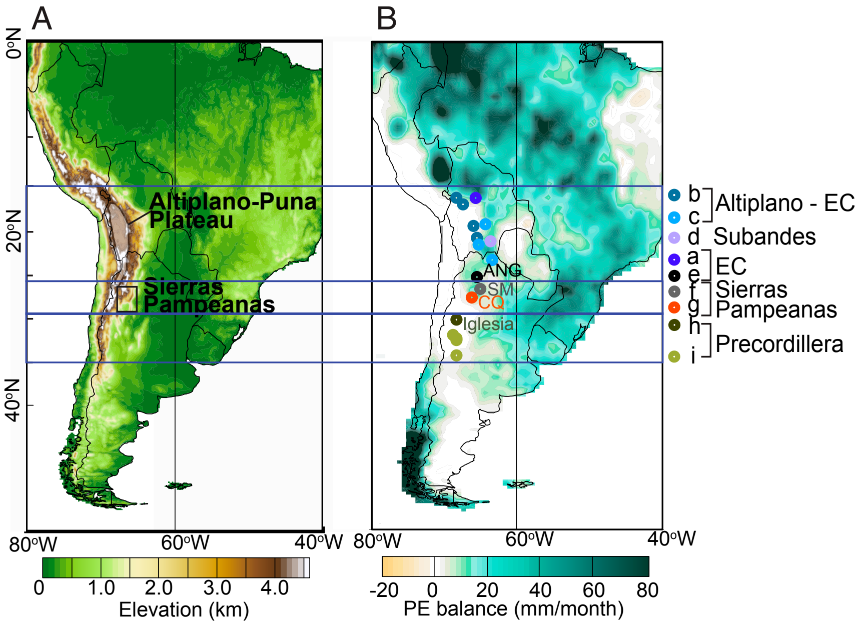

Fig. 1. (*A*) Ten-minute elevation map of South America. (*B*) Mean annual precipitation minus evaporation (PE balance) map with locations of stable isotope studies used in Figs. 2 and 3. Precipitation and evaporation are averaged over 1980–2000 period using data from Modern-Era Retrospective Analysis for research and applications project. (MERRA, ref. 56); with location of the basins used in this study (ANG, Angastaco; CQ, Porta Corral Quemado; SM, Santa Maria); proxies are from (a) (31); (b, c) (63, 64); (d) (36); (e) (27, 28, 33); (f) (37, 65); (g) (7); (h) (38); and (i) (66). Latitudinal bands used in Fig. 3 are indicated in purple.

pedogenic carbonate nodules are used as a proxy for variations of soil water $\delta^{18}O$ and $\delta^{13}C$, and hence carry information about hydroclimate and vegetation (17). Changes in soil water $\delta^{18}O$ are a function of elevation, moisture condition, moisture source, and rainout history (18). The $\delta^{13}C$ of pedogenic carbonate is a function of concentration and $\delta^{13}C$ of atmosphere CO_2, and $\delta^{13}C$ of soil respired CO_2. Variations of the latter is primarily dominated by the photosynthetic pathway favored by different plant species (C_3, C_4, or crassulacean acid metabolism photosynthesis) (19), which in turn is modulated by the environmental conditions experienced by plants during growth (20).

To evaluate hydroclimate sensitivity to changes in meridional SST structure, Andean uplift, and expansion of C_4 grasses, we carried out a suite of six prescribed SST experiments using a complex general circulation model ECHAM5-JSBACH-wiso (21–23) with Miocene boundary conditions (*Materials and Methods*). Due to the sparsity of SST estimates, an accurate meridional SST gradient for the interval of 10–7 Ma is unavailable (24). To cope with uncertainties in changes in SST gradients and CO_2, we conducted three sensitivity experiments sampling potential ranges of CO_2 decline and steepening of equator-to-pole SST gradient (EP-grad) from moderate (modCO_2, by 180 ppm; modGrad, by 5 °C) to a great magnitude (greatCO_2, by 280 ppm; greatGrad, by 7 °C) (3). Simulation results are reported as difference between sensitivity experiments and the control.

Results

Geochemical Record of Paleoenvironmental Changes in the Central Andes. In the central Andes, changes in oxygen isotopic compositions in the Miocene and Pliocene record are a result of changes in both surface elevation and coevolving regional climate and paleoenvironmental conditions (25–28). We selected records from sedimentary basins (Fig. 1) that achieved elevations and topography similar to modern largely before the LMC (29–31). Local topography was formed at different times due to the different tectono-morphic setting of the basins considered in this study (Fig. 1*B*). For example, structural, sedimentological, and thermochronological data from the Angastaco Basin, in the Eastern Cordillera (EC) of the central Andes, show that the local orographic barrier to the east of the basin was not uplifted until ~4 Ma (32), whereas the shift in stable isotope data occurs at ~6 Ma (33). Similarly, the range east of the Santa Maria Basin (Cumbre de Calchaquies) did not reach topography significant to act as an effective rain shadow before ~3 Ma (34). In general, local orographic effects are not expected to produce universal shifts in stable isotope values at the LMC boundary.

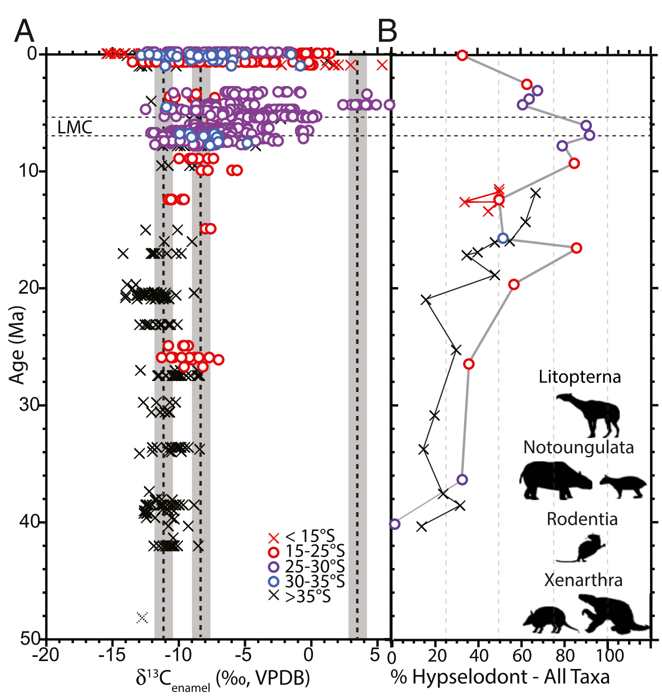

Fig. 2. Compilation of datasets for (*A*) fossil enamel $\delta^{13}C$ (12, 67) and (*B*) fossil crown height (69, 70) from South America. Symbols correspond to different specimens sampled from different latitudes within our region of interest (15–35°S) emphasized by the colored circles. Vertical dashed lines and gray bars identify the average and SDs in expected enamel $\delta^{13}C$ values for pure C_3 feeders (~−11/per mil), conservative upper limit for C_3 feeders in arid environments (~−8 per mil), and pure C_4 feeders (~+3.5 per mil), respectively (68). (*B*) Graph showing changes in the proportion of hypselodont (i.e., ever-growing teeth) taxa in different assemblages from northern, central, and southern Andes. The proportion of Elodont Mammalian Taxa at Fossil Localities in South America is presented in *SI Appendix*, Table S1.

$\delta^{18}O$ and $\delta^{13}C$ records are geographically grouped between 15 and 25°S, 25 and 30°S, and 30 and 35°S based on documented isotopic signatures for individual basins before (light color), during (medium color), and after the LMC (dark color) (Fig. 3). Under present-day conditions, the 15–35°S band features balanced precipitation minus evaporation (Fig. 1*B*), and mixed woodland and grassland ecosystems (35). $\delta^{18}O$ records from the Altiplano and northern sector of the EC, between 15 and 25°S, show an overall negative shift (Fig. 3). This shift is statistically significant at northern sites (17–18°S) on the Altiplano (Fig. 3*B*, one-way ANOVA, $P < 0.05$), where carbonate $\delta^{18}O$ values decrease by ~2‰ possibly reflecting a large drop in temperature (~10 °C) and surface uplift (26, 31). However, based on our climate simulations (shown later), this large drop is also attributable to the more ^{18}O-depleted moisture associated with the enhanced moist convection in the Intertropical convergence zone (ITCZ). Carbonate $\delta^{13}C$ values (Fig. 3*A*) show a clear increase of ~3‰ from pre-LMC to LMC in northern regions (17–18°S), which we attribute to enhanced aridity, reduced plant cover, and reduced soil respiration rates; these conditions would lead to a greater penetration of atmospheric CO_2 into soils, thereby increasing $\delta^{13}C$ values in pedogenic carbonates (18). Low-elevation records (Subandes) from 15 to 25°S imply a combined effect of cooling, more ^{18}O-depleted precipitation, and more variable climate conditions (36), although carbonates from other sites and post-LMC deposits are needed to generate a complete record of environmental response across this event.

Carbonate $\delta^{18}O$ values from all basins between 25 and 30°S (Fig. 3*D* and *SI Appendix*, Fig. S1) show universal positive shifts of ~2–3‰ (one-way ANOVA, $P < 0.05$). Nonetheless, these $\delta^{18}O$ values display large variability between records before the LMC, which likely documented strong seasonality and local environmental conditions (7). From pre-LMC to post-LMC, the $\delta^{13}C$ data from these basins (Fig. 3*C* and *SI Appendix*, Fig. S1) show strong variability and a general shift toward higher values during the LMC (one-way ANOVA, $P < 0.05$). The magnitude of this shift is highest in the north (~5‰, Angastaco Basin; Fig. 3*C*) and decreases to the south (~2‰, Santa Maria and Corral Quemado Basins; Fig. 3*C*). Post-LMC $\delta^{13}C$ values remain high except in the Santa Maria Basin where values drop to pre-LMC levels. The variability in $\delta^{13}C$ values may reflect seasonal precipitation patterns (and local paleotoporaphy) in each basin being distinct enough to generate appreciable differences in floral composition (i.e., C_3-C_4 abundance). The positive shift in $\delta^{13}C$ values likely reflects an increase in aridity and expansion of C_4 plants, which is more pronounced in central EC basins. The $\delta^{13}C$ values were high south of 25°S even before the LMC, indicating overall dry conditions and presence of C_4 grasses as supported by high $\delta^{13}C$ values (>−8.0‰) of fossil tooth enamel (Fig. 2*A*) from several different clades of herbivorous South American mammals (7, 33, 37). In the Corral Quemado Basin, C_4 grasses or open, arid habitats were likely widespread and persistent during the LMC (Fig. 2 *C* and *E*), and expanded after

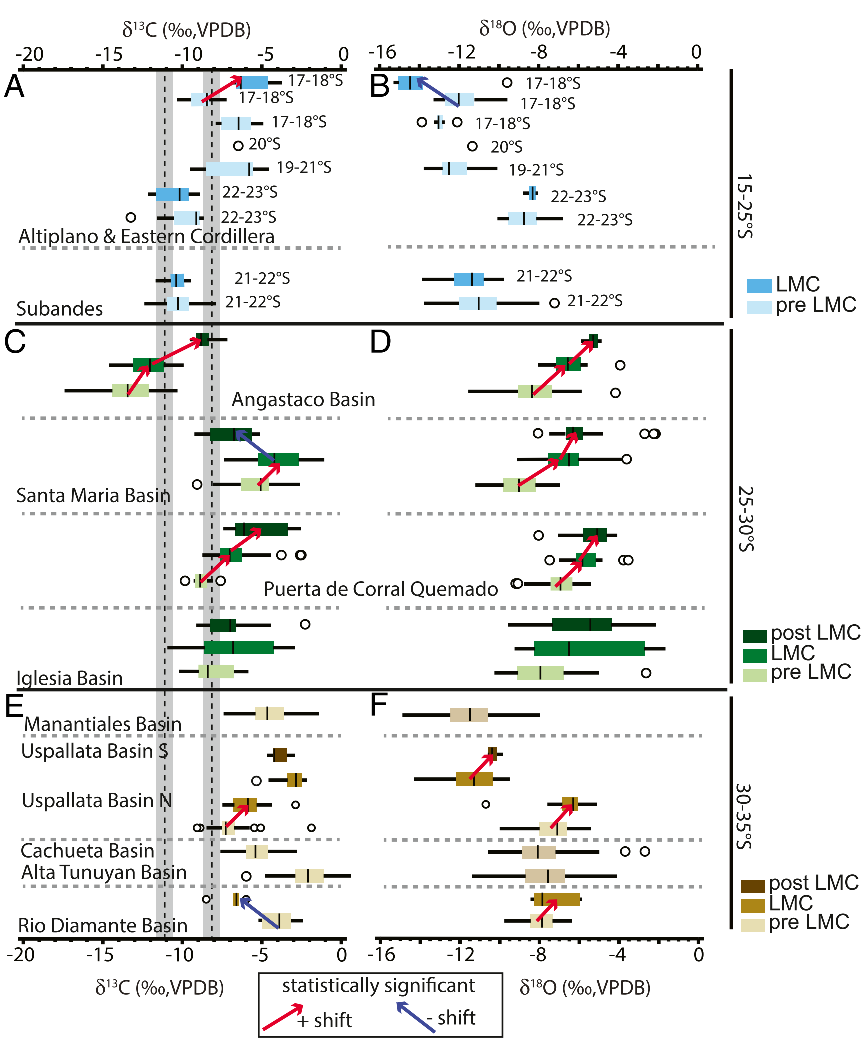

Fig. 3. Boxplots of carbon (*A*, *C*, and *E*) and oxygen (*B*, *D*, and *F*) isotope data for pedogenic carbonates from localities in Bolivia (15–23°S) and Argentina (25–35°S). Red arrow: statistically significant positive shift; blue arrow: statistically significant negative shift (Dataset S1). Boxes define the distribution of data, marking the upper (+25%) and lower (−25%) quartiles, with a vertical line within each box marking the median of the population. The width of the box defines the interquartile distance (IQD). Horizontal lines extending from each box mark max and min values falling within 1.5× the IQD beyond the upper and lower quartiles; any points exceeding this range (outliers) are plotted as circles. Within the basins or locations sampled from the three selected latitudinal ranges (15–20°S, 25–30°S, 32–35°S), data are binned into samples preceding the LMC (lightest color, 7–9 Ma), during the LMC (middle color, 5–7 Ma), and after the LMC (darkest color, 5–3 Ma). For samples from Bolivia and basins to the south, records covering the entire before, during, and after the LMC interval are not available. Vertical dashed line and gray-shaded bar behind it define a conservative estimated cutoff (−8.2‰) and ±1σ (0.6‰) between floras composed of 100% C_3 plants (arid-adapted) versus those floras that include an appreciable amount of C_4 plants for the interval from 20 Ma to present (mean and 1σ calculated from Supplementary Dataset S1 in ref. 68).

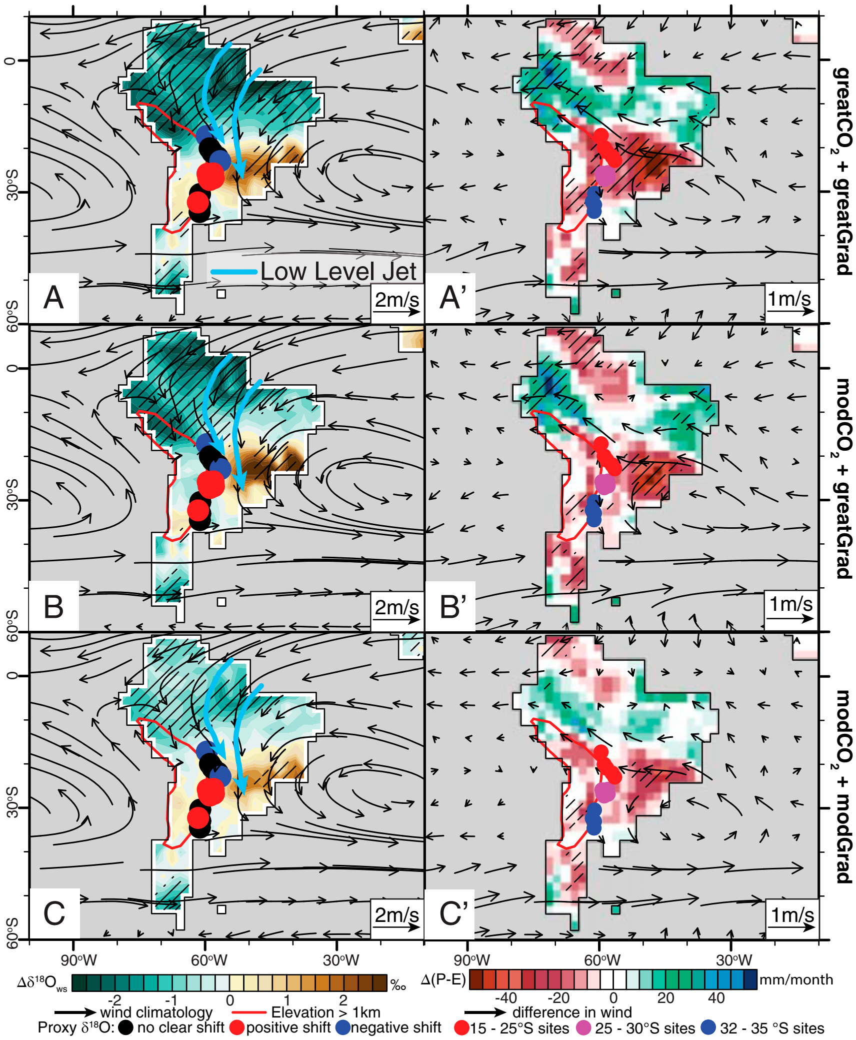

Fig. 4. Austral summer (December to February) 850-hPa circulation climatology, and changes in soil water $\delta^{18}O$ due to enhanced equator-to-pole SST gradient and CO_2 decline during the LMC (*A*–*C*). (A′–C′): the same as *A*–*C*, but for Δ(P-E) and circulation changes from the control pre-LMC simulation. Proxy carbonate $\delta^{18}O$ shifts are colored in A to C by red: positive, blue: negative, white: no clear signal. Proxy site locations are colored with latitudes: red: 15–25°S, magenta: 25–30°S, and blue: 32–35°S. Hatched areas show differences from the control case significant at $P < 0.1$.

the LMC at ∼4 Ma (7, 37), potentially attributable to an increase in summer-dominated rainfall (7). Although data from the Iglesia Basin are scattered, sedimentology and paleopedology suggest generally semiarid conditions during the Late Miocene, with slightly more humid conditions between ∼9.5 and 7 Ma (38) before the LMC, and then transitioning toward more arid conditions during the LMC. $\delta^{13}C$ values were high since ∼19 Ma (>−8‰) and increased slightly during the LMC, suggesting the predominance and possibly a small expansion of C_4 plants or arid, open habitats between 7 and 4.5 Ma (37).

Basins from 30 to 35°S (Fig. 1*B*) show $\delta^{18}O$ and $\delta^{13}C$ values typical of dry conditions since the Early Miocene (Fig. 3 *E* and *F* and *SI Appendix*, Fig. S1) with high $\delta^{13}C$ values suggesting a substantial amount of C_4 grasses in the ecosystem. Both $\delta^{18}O$ and $\delta^{13}C$ values show little change across LMC, indicating fairly stable hydroclimate and grassland ecosystems. These basins may have already been arid and had an abundance of C_4 vegetation or open habitats before the LMC. Palynological samples from sites in northern Argentina (25 to 35°S) support this trend, showing spatial variation with lower diversity and a greater number of open-habitat and xerophytic species (Poaceae, Asteraceae, Fabacea) to the south and much higher diversity of forest-indicator taxa (Podocarpaceae, Nothofagaceae) to the north and east (39). Over time, pollen records show a transition from riparian forests and grasslands in the Early and Middle Miocene to seasonally dry forests and savannas during the Pliocene and Pleistocene (39).

Simulated South America Climate Changes Across LMC. On land, annual mean changes in precipitation minus evaporation [Δ(P-E)] shows small increases induced by different ranges of cooling at the LMC (7% in modCO2 + modGrad, and 11% in both modCO2 + greatGrad and greatCO2 + greatGrad) (*SI Appendix*, Fig. S4 *A*–*C*) yet with strong heterogeneity attributable to individual or combined influences from land–sea thermal contrast, distribution of topography, and stationary wave propagation (40). Increase in annual mean Δ(P-E) is a combined effect of reduction of evaporation by 3–5%, and increase in precipitation by 4–7% primarily in response to changes in EP-grad. Across South America, Δ(P-E) is the strongest during the austral summer (December to February) with net surplus across the Amazon Basin and deficit to the south and southeastern side (Fig. 4 *A*–*C*). This austral summer moisture deficit results from reduction in moisture transport from tropical Amazon and tropical Atlantic toward subtropics (Fig. 4, left column), following changes in 850 hPa circulation (Fig. 4, right column). This reduction can be explained by the weakening of the South American low-level jet (Fig. 4 *A*′–*C*′). Corresponding to Δ(P-E), simulated soil water $\delta^{18}O$ ($\delta^{18}O_{sw}$) values decrease between 15 and 25°S, and increase in the subtropics between 25 and 35°S. This pattern magnifies with greater increase in EP-grad.

Uplift of the Andes leads to increase in summer precipitation and P-E across the Andes and southern Brazil, but decrease of summer precipitation and P-E northward, reflecting the southwestward migration of the moist convection attributable to the enhancement of the South American low-level jet (41, 42) (*SI Appendix*, Fig. S3). However, this hydroclimate response is associated with widespread negative soil water $\delta^{18}O$ shift across the subtropical South America, which cannot explain the proxy records. In contrast, we simulate a negative shift in summer P-E, and a positive shift in soil water $\delta^{18}O$ in the southern Brazil and central Andes in response to the replacement of forests with grassland across subtropical South America (*SI Appendix*, Fig. S3). This shift is indicative of the positive feedback between rain band–desert boundary, and forest–grassland surface albedo contrast, reminiscent of the vegetation-regional atmospheric circulation coupling proposed for the Sahel–Sahara region (43).

Evidence for Changes in Hydroclimate Associated with Hadley Circulation Strengthening. Sensitivity experiments with different magnitudes of CO_2 decline and steepening of EP-grad show enhanced precipitation surplus and moisture convergence toward the ITCZ and midlatitude storm track, but enhanced precipitation deficit and moisture divergence from subtropics; Δ(P-E) and circulation changes suggest strengthened Hadley circulation (HC) on annual and austral summer average (*SI Appendix*, Figs. S4 and S5). Based on the consistency between proxy carbonate $\delta^{18}O$ shifts across the LMC between 15 and 35°S and simulated spatial pattern of $\delta^{18}Osw$ changes during austral summer across the same region (Fig. 4), we suggest that proxy carbonate $\delta^{18}O$ shifts likely reflect strengthened HC, epitomized in South America by an enhanced ITCZ and subtropical aridification. Our conclusion is also based on the known seasonal preference of soil carbonate formation. Soil carbonate typically forms during rapid degassing of CO_2 from soil water, which occurs primarily during warm and dry periods of the year (44). Hence, simulated austral summer $\delta^{18}Osw$ changes are likely more representative of changes in proxy carbonate $\delta^{18}O$ records.

Discussion

Our study highlights the importance of global climate changes on Late Miocene stable isotope proxies from the central Andes, instead of simply changes in topography and elevation. The HC strengthening can explain the ecosystem transition at the LMC aided with CO_2 decline and vegetation albedo–regional circulation coupling. The subtropical aridification of South America may favor more drought-tolerant C_4 plants compared with C_3 plants. This advantage of C_4 plants can be further amplified by vegetation–regional circulation coupling, which is shown to enhance aridity at the forest–grassland transition when subtropical forests are replaced with grasses in our experiment (*SI Appendix*, Fig. S3). CO_2 fertilization may have also supported pre-LMC forest environment (45), and the efficiency of C_4 photosynthesis over C_3 photosynthesis under low-CO_2 conditions [up to 250 ppm (46)] could have accelerated the ecosystem transition toward C_4 plants in response to CO_2 decline.

Our finding contrasts with the CO_2 driven hydrological changes proposed for present-day and near-future climate; rising CO_2 is thought to cause tropospheric moistening and enhance the present-day P-E pattern (and hence subtropical drying) especially across the ocean assuming negligible contributions from atmospheric circulation change (47). Instead, we found that low-carbonate $\delta^{18}O$ across subtropical South America before LMC supports a wetter subtropical South America dominated by C_3 grasses under a warm and potentially higher CO_2 climate. Consistent with a recent study (48), we suggest that hydroclimate changes at geological timescale such as the LMC are likely driven by atmospheric circulation changes, rather than fast CO_2 radiative forcing or uniform SST warming, which are likely more important to transient hydroclimate responses to rising CO_2 (41, 49). In our simulations, enhanced meridional atmosphere circulation reflects increase of atmospheric heat transport induced by increase of EP-grad. Proxy records from South America support this enhancement during the LMC, and hence, the potentially positive relationship between EP-grad and HC strength at geological timescale (50). This relationship implies weaker HCs during warm climates with low EP-grad, which could have played an important role in continental greening during periods such as Eocene (51) and Pliocene (52). Recent studies suggest that this shallow EP-grad may be related to marine stratocumulus clouds. A large reduction in subtropical-midlatitude cloud albedo results in large warming across the corresponding ocean area, and hence a relaxed EP-grad (48, 52). Weaker HC subsidence due to a low EP-grad may further lower the cloud albedo across marine stratocumulus region by relaxing the boundary layer inversion. This process implies a positive feedback among EP-grad, HC strength, and marine cloud albedo. Recent HC expansion has been partially attributed to changes in shortwave cloud-cooling effect in the midlatitudes (53). However, simulating low cloud feedbacks to SST warming remains challenging (54), and changes in the strength of HC (55) remain equivocal.

Strengthening of the HC during the LMC is supported by biotic responses, which show increasing adaptation to arid environments with a northward progression over time. As with earlier records from Patagonia (14, 56), pollen and phytolith evidence attests to a complex and dynamic flora that was responsive to major changes in global climate. Although increasing evidence has shown that the evolution of high-crowned teeth by herbivorous mammals may not have been directly tied to the expansion of grasslands (14, 57), the early appearance of this trait in high-latitude faunas of South America supports an association between hypsodonty and arid, open environments. Acquisition of high-crowned teeth by these taxa means they would have benefited from the expansion of arid habitats at the LMC and would have been primed to take advantage of the increased abundance of C_4 grasses in the Late Miocene.

Materials and Methods

Stable isotope data used to compile Fig. 3 are available in Dataset S1. We run the ECHAM5-JSBACH-wiso model (23, 58) at 2° horizontal resolution with 31 vertical atmospheric levels from surface to 10 hPa. The control experiment utilizes published Miocene boundary conditions (topography, geography, and vegetation) (59–62), 560 ppm CO_2, and monthly SST climatologies matching the reconstructed Miocene global meridional SST gradient estimated for the interval of 17–11 Ma (*SI Appendix*). The sensitivity experiments feature moderate CO_2 decline by 160 ppm and moderate enhancement of equator-to-pole SST gradient (EP-grad) from the control of ∼5 °C around the poles by a maximum of 5 °C around the poles (modCO2 + modGrad), a moderate CO_2 decline by 160 ppm and greater enhancement of EP-grad by a maximum of 7 °C around the poles (modCO2 + greatGrad), and a greater CO_2 decline by 280 ppm and greater enhancement of EP-grad by 7 °C (greatCO2 + greatGrad) (*SI Appendix*). In addition, two sensitivity experiments are carried out to feature end members of rapid Andean uplift from ∼1.5 to ∼3 km at grid-mean model resolution and subtropical grassland expansion (*SI Appendix*). Reported results are shown as differences between the sensitivity and control run. Climatologies are calculated for the last 30 y of a total of 40 model-year simulation for each experiment.

ACKNOWLEDGMENTS. We thank J. Quade for useful discussions and constructive feedback during preparation of this manuscript, three anonymous reviewers, and the editor for constructive criticism which helped improve this work. High-performance computing support from Cheyenne (doi:10.5065/D6RX99HX) provided by NCAR's Computational and Information Systems Laboratory was sponsored by NSF-integrated Earth System program (Grant 1814029) (to R.F.).

1. Beerling DJ, Fox A, Stevenson DS, Valdes PJ (2011) Enhanced chemistry-climate feedbacks in past greenhouse worlds. *Proc Natl Acad Sci USA* 108:9770–9775.
2. Londoño L, et al. (2018) Early Miocene CO_2 estimates from a Neotropical fossil leaf assemblage exceed 400 ppm. *Am J Bot* 105:1929–1937.
3. Herbert TD, et al. (2016) Late Miocene global cooling and the rise of modern ecosystems. *Nat Geosci* 9:843–847.
4. Pagani M, Freeman KH, Arthur MA (1999) Late miocene atmospheric CO(2) concentrations and the expansion of C(4) grasses. *Science* 285:876–879.

5. Fedorov AV, et al. (2013) Patterns and mechanisms of early Pliocene warmth. *Nature* 496:43–49.
6. DeCelles PG, et al. (2015) *Cyclical Orogenic Processes in the Cenozoic Central Andes Geodynamics Of a Cordilleran Orogenic System: The Central Andes of Argentina and Northern Chile*, eds DeCelles PG, Ducea MN, Carrapa B, Kapp PA (Geological Society of America Memoir, New York), Vol 212.
7. Latorre C, Quade J, McIntosh WC (1997) The expansion of C-4 grasses and global change in the late Miocene: Stable isotope evidence from the Americas. *Earth Planet Sci Lett* 146:83–96.
8. Cerling TE, et al. (1997) Global vegetation change through the Miocene/Pliocene boundary. *Nature* 389:153–158.
9. MacFadden BJ, Cerling TE, Prado J (1996) Cenozoic terrestrial ecosystem evolution in Argentina: Evidence from carbon isotopes of fossil mammal teeth. *Palaios* 11: 319–327.
10. MacFadden BJ, Wang Y, Cerling TE, Anaya F (1994) South American fossil mammals and carbon isotopes: A 25 million-year sequence from the Bolivian Andes. *Palaeogeogr Palaeoclimatol Palaeoecol* 107:257–268.
11. Janis CM, Damuth J, Theodor JM (2002) The origins and evolution of the North American grassland biome: The story from the hoofed mammals. *Palaeogeogr Palaeoclimatol Palaeoecol* 177:183–198.
12. Kohn MJ, Wieland MS, Parkinson CD, Upreti BN (2015) Quasi-static Eocene–Oligocene climate in Patagonia promotes slow faunal evolution and mid-Cenozoic global cooling. *Palaeogeogr Palaeoclimatol Palaeoecol* 435:24–37.
13. Dunn RE, Strömberg CAE, Madden RH, Kohn MJ, Carlini AA (2015) Linked canopy, climate, and faunal change in the Cenozoic of Patagonia. *Science* 347:258–261.
14. Strömberg AE (2008) Evolution of grasses and grassland ecosystems. *Annu Rev Earth Planet Sci* 39:517–544.
15. Zachos J, Pagani M, Sloan L, Thomas E, Billups K (2001) Trends, rhythms, and aberrations in global climate 65 Ma to present. *Science* 292:686–693.
16. Cerling TE, Quade J (1993) Stable carbon and oxygen isotopes in soil carbonates. *Climate Change in Continental Isotopic Records*, eds Swart PK, Lohmann KC, McKenzie J, Savin S (American Geophysical Union, Washington, DC), Monograph 78, pp 217–231.
17. Cerling TE (1999) Stable carbon isotopes in palaeosol carbonates. *Palaeoweathering, Palaeosurfaces and Related Continental Deposits*, International Association of Sedimentologists Special Publication, eds Thiry M, Simon-Coinçon R (Blackwell Sci, Oxford), Vol 27, pp 43–60.
18. Cerling TE (1984) The stable isotopic composition of modern soil carbonate and its relationship to climate. *Earth Planet Sci Lett* 71:229–240.
19. O'Leary MH (1981) Carbon isotope fractionation in plants. *Phytochemistry* 20: 553–567.
20. Körner C, Farquhar GD, Wong SC (1991) Carbon isotope discrimination by plants follows latitudinal and altitudinal trends. *Oecologia* 88:30–40.
21. Feng R, Poulsen CJ, Werner M (2016) Tropical circulation intensification and tectonic extension recorded by Neogene terrestrial d18O records of the western United States. *Geology* 11:971–974.
22. Haese B, Werner M, Lohmann G (2013) Stable water isotopes in the coupled atmosphere–land surface model ECHAM5-JSBACH. *Geosci Model Dev* 6:1463–1480.
23. Werner M, Langebroek PM, Carlsen T, Herold M, Lohmann G (2011) Stable water isotopes in the ECHAM5 general circulation model: Toward high-resolution isotope modeling on a global scale. *J Geophys Res* 116:D15109.
24. Micheels A, Bruch AA, Uhl D, Utescher T, Mosbrugger V (2007) A Late Miocene climate model simulation with ECHAM4/ML and its quantitative validation with terrestrial proxy data. *Palaeogeogr Palaeoclimatol Palaeoecol* 253:251–270.
25. Madden RH (2014) *Hypsodonty in Mammals* (Cambridge University Press, Cambridge, UK).
26. Garzione CN, et al. (2017) The tectonic evolution of the central Andean plateau and geodynamic implications for the growth of plateaus. *Annu Rev Earth Planet Sci* 45: 529–559.
27. Quade J, et al. (2015) The growth of the central Andes, 22°S–26°S. *Geol Soc Am Mem* 12:277–308.
28. Rohrmann A, et al. (2016) Miocene orographic uplift forces rapid hydrological change in the southern central Andes. *Sci Rep* 6:35678.
29. Canavan RR, et al. (2014) Early Cenozoic uplift of the Puna Plateau, Central Andes, based on stable isotope paleoaltimetry of hydrated volcanic glass. *Geology* 42: 447–450.
30. Carrapa B, et al. (2014) Uplift of the Central Andes of NW Argentina associated with upper crustal shortening, revealed by multiproxy isotopic analyses. *Tectonics* 33: 1039–1054.
31. Leier A, McQuarrie N, Garzione C, Eiler J (2013) Stable isotope evidence for multiple pulses of rapid surface uplift in the Central Andes, Bolivia. *Earth Planet Sci Lett* 371–372:49–58.
32. Carrapa B, Bywater-Reyes S, DeCelles PG, Mortimer E, Gehrels GE (2012) Late Eocene-Pliocene basin evolution in the Eastern Cordillera of northwestern Argentina (25 degrees-26 degrees S): Regional implications for Andean orogenic wedge development. *Basin Res* 24:249–268.
33. Bywater-Reyes S, Carrapa B, Clementz M, Schoenbohm L (2010) Effect of late Cenozoic aridification on sedimentation in the Eastern Cordillera of northwest Argentina (Angastaco basin). *Geology* 38:235–238.
34. Sobel E, Strecker MR (2003) Uplift, exhumation and precipitation: Tectonic and climatic control of late cenozoic landscape evolution in the northern Sierras Pampeanas, Argentina. *Basin Res* 15:431–451.
35. Hansen MC, DeFries RS, Townshend JR, Sohlberg R (2000) Global land cover classification at 1 km spatial resolution using a classification tree approach. *Int J Remote Sens* 21:1331–1364.
36. Mulch A, Uba CE, Strecker MR, Schoenberg R, Chamberlain CP (2010) Late Miocene climate variability and surface elevation in the central Andes. *Earth Planet Sci Lett* 290:173–182.
37. Cotton JM, Hyland EG, Sheldon ND (2014) Multi-proxy evidence for tectonic control on the expansion of C4 grasses in northwest Argentina. *Earth Planet Sci Lett* 395: 41–50.
38. Ruskin BG, Jordan TE (2007) Climate change across continental sequence boundaries: Paleopedology and lithofacies of Iglesia Basin, northwestern Argentina. *J Sediment Res* 77:661–679.
39. Garralla SS, Anzótegui LM, Mautino LR (2016) Relaciones paleoflorísticas del Mioceno–Plioceno del norte argentino. *Publicación Electrónica de la Asociación Paleontológica Argentina* 16:1–13.
40. He J, Soden BJ (2015) Anthropogenic weakening of the tropical circulation: The relative roles of direct CO2 forcing and sea surface temperature change. *J Clim* 28: 8728–8742.
41. Insel N, Poulsen CJ, Ehlers TA (2010) Influence of the Andes Mountains on South American moisture transport, convection, and precipitation. *Clim Dyn* 35:1477–1492.
42. Lenters JD, Cook KH (1995) Simulation and diagnosis of the regional summertime precipitation climatology of South America. *J Clim* 8:2988–3005.
43. Charney JG (1975) Dynamics of deserts and drought in Sahel. *Q J R Meteorol Soc* 1975: 193–202.
44. Breecker DO, Sharp ZD, McFadden LD (2010) Atmospheric CO2 concentrations during ancient greenhouse climates were similar to those predicted for A.D. 2100. *Proc Natl Acad Sci USA* 107:576–580.
45. Zhu Z (2016) Greening of the earth and its drivers. *Nat Clim Chang* 6:791–795.
46. Gerhart LM, Ward JK (2010) Plant responses to low [CO2] of the past. *New Phytol* 188: 674–695.
47. Held IM, Soden BJ (2006) Robust responses of the hydrological cycle to global warming. *J Clim* 19:5686–5699.
48. Burls NJ, Fedorov AV (2017) Wetter subtropics in a warmer world: Contrasting past and future hydrological cycles. *Proc Natl Acad Sci USA* 114:12888–12893.
49. He J, Soden BJ (2017) A re-examination of the projected subtropical precipitation decline. *Nat Clim Chang* 7:53–57.
50. Rind D, Perlwitz J (2004) The response of the Hadley circulation to climate changes, past and future. *The Hadley Circulation: Present, Past and Future* (Springer, Dordrecht, The Netherlands).
51. Greenwood DR, Wing SL (1995) Eocene continental climates and latitudinal temperature gradients. *Geology* 23:1044–1048.
52. Burls NJ, Fedorov AV (2014) Simulating Pliocene warmth and a permanent El Niño-like state: The role of cloud albedo. *Paleoceanography* 29:893–910.
53. Ceppi P, Hartmann DL (2016) Clouds and the atmospheric circulation response to warming. *J Clim* 29:783–799.
54. Schneider T, et al. (2017) Climate goals and computing the future of clouds. *Nat Clim Chang* 7:3–5.
55. Feng R, Li J, Wang J (2011) Regime change of the boreal summer Hadley circulation and its connection with the tropical SST. *J Clim* 24:3867–3877.
56. Palazzesi L, Barreda V (2012) Fossil pollen records reveal a late rise of open-habitat ecosystems in Patagonia. *Nat Commun* 3:1294.
57. Jardine PE, Janis CM, Sahney S, Benton MJ (2012) Grit not grass: Condordant patterns of early origin of hypsodonty in Great Plains ungulates and glires. *Palaeogeogr Palaeoclimatol Palaeoecol* 1:365–366.
58. Roeckner E, et al. (2003) *The Atmospheric General Circulation Model ECHMAM5, Part I* (Max Plank Institute, Hamburg, Germany).
59. Feng R, et al. (2013) Early Cenozoic evolution of topography, climate, and stable isotope in precipitation in the North American Cordillera. *Am J Sci* 313:613–648.
60. Goldner A, Herold N, Huber M (2014) The challenge of simulating the warmth of the mid-Miocene climatic optimum in CESM1. *Clim Past* 10:523–536.
61. Herold N, Huber M, Müller RD, Seton M (2012) Modeling the Miocene climatic optimum: Ocean circulation. *Paleoceanography* 27:PA1209.
62. Herold N, Seton M, Müller RD, You Y, Huber M (2008) Middle Miocene tectonic boundary conditions for use in climate models. *Geochem Geophys Geosyst* 9:Q10009.
63. Garzione CN, et al. (2014) Clumped isotope evidence for diachronous surface cooling of the Altiplano and pulsed surface uplift of the Central Andes. *Earth Planet Sci Lett* 393:173–181.
64. Garzione CN, et al. (2008) Rise of the Andes. *Science* 320:1304–1307.
65. Kleinert K, Strecker MR (2001) Changes in moisture regime and ecology in response to late Cenozoic orographic barriers: The Santa Maria valley, Argentina. *Geol Soc Am Bull* 113:728–742.
66. Hoke GD, Giambiagi LB, Garzione CN, Mahoney JB, Strecker MR (2014) Neogene paleoelevation of intermontane basins in a narrow, compressional mountain range, southern Central Andes of Argentina. *Earth Planet Sci Lett* 506:143–164.
67. Hynek SA, et al. (2012) Small mammal carbon isotope ecology across the Miocene–Pliocene boundary, northwestern Argentina. *Earth Planet Sci Lett* 321–322:177–188.
68. Passey BH, et al. (2009) Strengthened East Asian summer monsoons during a period of high-latitude warmth? Isotopic evidence from Mio-Pliocene fossil mammals and soil carbonates from northern China. *Earth Planet Sci Lett* 277:443–452.
69. Marshall LG, Patterson B (1981) *Geology and Geochronology of the Mammal-Bearing Tertiary of the Valle de Santa María and Río Corral Quemado, Catamarca Province, Argentina* (Field Museum of Natural History, Chicago, IL).
70. Zimicz N, Payrola P, del Papa C (2018) New, Late Miocene mammalian assemblage from the Palo Pintado Formation (Northwestern Argentina). *Journal of South American Earth Sciences* 81:31–44.